Supplementary Information

First structural characterization of Pa(IV) in aqueous solution and quantum chemical investigations of the tetravalent actinides up to Bk(IV): the evidence of a curium break

Nidhu lal Banik,[a]* Valérie Vallet,[b] Florent Réal,[b] Réda Mohamed Belmecheri,[c] Bernd Schimmelpfennig,[a] Jörg Rothe,[a] Remi Marsac,[a] Patric Lindqvist-Reis,[a] Clemens Walther,[d] Melissa A. Denecke,[e] and Christian M. Marquardt[a]

[a] Dr. N. L. Banik, Dr. B. Schimmelpfennig, Dr. J. Rothe, Dr. R. Marsac, Dr. P. Lindqvist-Reis, Dr. C. M. Marquardt, Institut für Nukleare Entsorgung, Karlsruhe Institute of Technology, P.O. Box 3640, 76021 Karlsruhe (Germany)
E-mail: nidhu.banik@kit.edu

[b] Dr. V. Vallet, Dr. F. Réal
Laboratoire PhLAM, UMR-CNRS 8523, Université Lille 1 (Sciences et Technologie), F-59655 Villeneuve d'Ascq, France
E-mail: valerie.vallet@univ-lille1.fr

[c] Dr. R. M. Belmecheri
Laboratoire de Thermodynamique et Modélisation Moléculaire, Faculté de Chimie, USTHB BP 32 El-Alia, 16111 Bab-Ezzouar, (Algeria)

[d] Prof. Dr. C. Walther
Institut für Radioökologie und Strahlenschutz. Leibniz Universität Hannover, Hannover (Germany)

[e] Prof. Dr. M. A. Denecke
Dalton Nuclear Institute, The University of Manchester, Manchester (UK)

List of Contents:

1 Experimental Section

1.1 Samples and experimental conditions

All experiments were performed with ^{231}Pa, the only long-lived naturally occurring isotope of protactinium (half-life 3.276×10^4 yr). Protactinium hydride, available from a batch originating from earlier activities at the former Kernforschungzentrum Karlsruhe (presently ITC-CPV (KIT)), was dissolved in strong acid (HNO_3 or HCl > 6 M). The separation of ^{231}Pa from its daughters ^{227}Ac, ^{227}Th and ^{223}Ra was performed by ion-exchange chromatography. The activity and purity of ^{231}Pa were verified by α and γ spectrometry. The concentration of ^{231}Pa in solution was measured by liquid scintillation counting (LSC) throughout the experiments. For reduction of Pa(V) to Pa(IV) two different reduction agents were used and their efficiency were evaluated. Rongalite ($Na^+HOCH_2SO_2^-$) as a reducing agent reduced Pa(V) to Pa(IV) more efficiently and stabilized the reduced species in solution for a longer time period than did the zinc-mercury amalgam (see article for details). To avoid oxidation by oxygen, all experiments were performed in an argon-filled glove box (O_2 < 5 ppm) at room temperature. Preparative and spectroscopic studies with Pa(IV) were performed at concentrations between $2.0\cdot10^{-6}$ and $3.0\cdot10^{-4}$ M using rongalite at a concentration between 0.01 M and 0.0001 M. Optimal stability was obtained at Pa(IV) and rongalite concentrations of $1.2\cdot10^{-5}$ and 0.0001 M, respectively. At this condition the solution still contained 98% Pa(IV) 5 days and ~ 70 % Pa(IV) 14 days after preparation. The oxidized Pa(V) formed colloids over time. The oxidation states of Pa(V) and Pa(IV) in stock and sample solutions were investigated by UV-vis absorption spectroscopy and time-resolved laser induced spectroscopy; see below.

1.2 UV-vis absorption spectroscopy

Absorption spectra of the solutions were recorded in 1 cm quartz cuvettes (Hellma) with a Cary 5 (Varian) UV-Vis-NIR spectrophotometer in the range 200-600 nm with a steps size 0.2 nm.

Consistent with literature data,[1] the absorption spectrum of Pa(V) shows no pronounced bands but a featureless, monotonous increase of the absorption to shorter wavelengths in the region 210-350 nm. However, three absorption bands at 225, 256 and 278 nm emerged after treatment of the Pa(V) solution with Zn-Hg amalgam (Figure 1). These bands originate from Pa(IV) $5f^1$–$6d^1$ transitions. Their positions and the intensities vary slightly with the type and the concentration of the acid. Typically, the bands shift to longer wavelength with increasing concentration and complexation strength of the anions of the acid. This agrees with pioneer absorption spectroscopic studied on Pa(IV) in perchloric, hydrochloric, and sulfuric acid solutions.[2] As mentioned in the article, rongalite is superior over Zn-Hg amalgam in that it stabilizes Pa(IV) for a longer time than does Zn-Hg amalgam. We found no evidence that it binds to Pa(IV). However, the rather strong absorption band of rongalite at ~284 nm masks the absorption spectrum of Pa(IV) (Fig. S1).

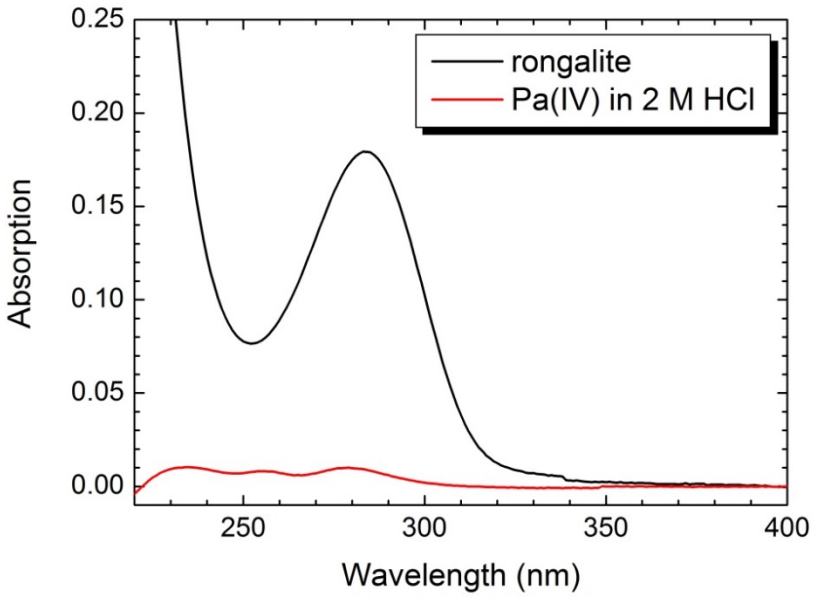

Fig. S1. Absorption spectra of $5 \cdot 10^{-4}$ M rongalite in water (black curve) and $1 \cdot 10^{-5}$ M Pa(IV) prepared by Zn-Hg amalgam in 2 M aqueous hydrochloric acid solution (red curve).

1.3 Time-resolved laser fluorescence spectroscopy (TRLFS)

A Nd:YAG laser combined with a OPO-SL (Spectra-Physics Laser, Inc., Mountain View, CA) as excitation source, a spectrograph (Acton Research SpectraPro 300i, Acton, MA), and an intensified CCD camera (PicoStar HR, LaVision, Inc., Göttingen, Germany) were used to record TRLFS emission spectra of Pa(IV). The laser system operates at wavelengths between 220 and 1800 nm. A flash lamp-pumped Nd:YAG laser generates laser pulses of 1064 nm wavelength.[3] The output energy averages 1300 mJ per pulse; the pulse width is ~10 ns with a pulse-to-pulse stability of ± 2%. By directing the laser through several non-linear optical devices, 2nd and 3rd harmonics are generated and laser pulses leave the Nd:YAG with a pulse width of 8 ns at a wavelength of 355 nm. Approximately 80% of the laser beams are channeled directly into the power oscillator (PO). The remaining 20% are directed into the master oscillator (MO), where the desired wavelength is created by double-pumping a BBO crystal. The laser excitation wavelength was set to 245 nm. The temperature was 21 ± 1 ºC. The laser beam was directed into a quartz cuvette with 1 cm path length. All spectra were baseline-corrected. Luminescence lifetimes were obtained by recording of emission spectra (380-540 nm) at different delay times up to 100 ns; the areas of the spectra were plotted vs. the delay time to provide the luminescence decay time (k) and thus the luminescence lifetime ($\tau = 1/k$). The spectra were analyzed using Origin™ (version 7.5, OriginLab Corporation).

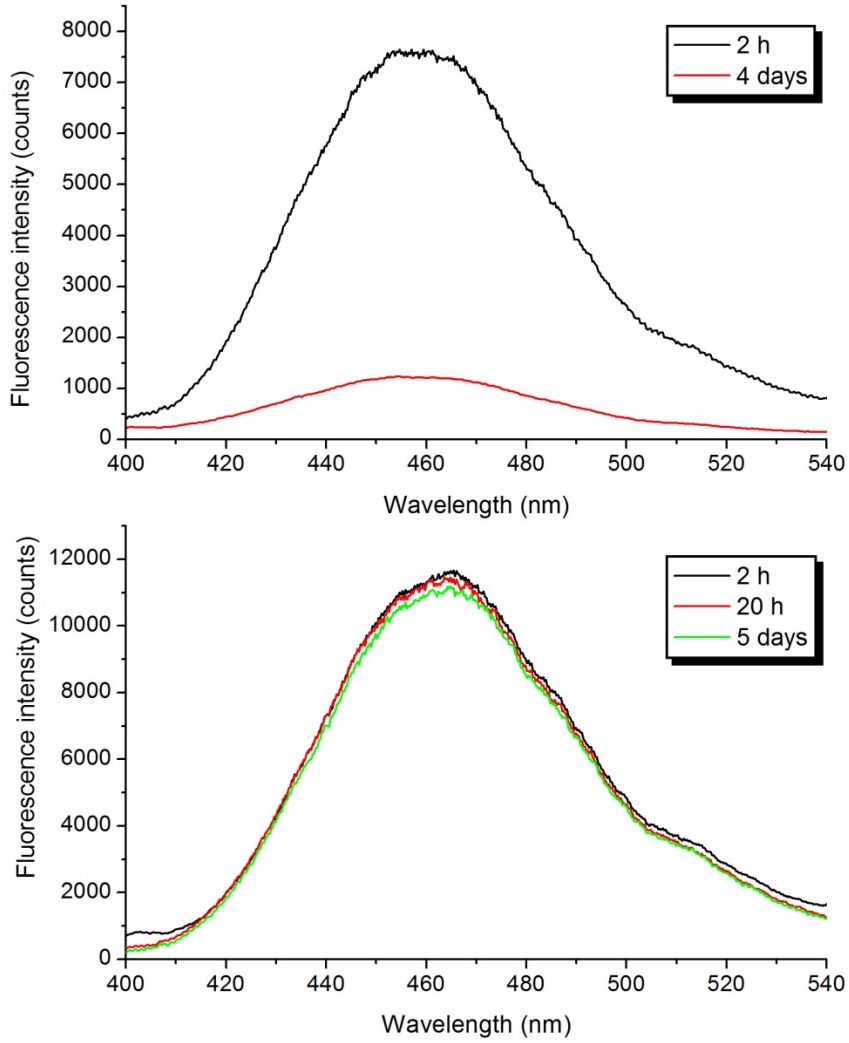

Figure S2. TRLFS spectra of $1 \cdot 10^{-5}$ M Pa(IV) in 6.0 M H_2SO_4 using Zn-Hg amalgam as reducing agent (top) and $5 \cdot 10^{-4}$ M rongalite as reducing agent (bottom).

Rongalite does not exhibit a luminescence band in the nanosecond regime. Thus, we used TRLFS to study the luminescence of Pa(IV) and its redox stability in the rongalite-containing solutions. For TRLFS, laser excitation (245 nm) into the 6d levels resulted in a broad $6d^1$–$5f^1$ emission band at ~465 nm in perchloric acid and ~455 nm in hydrochloric and sulfuric acid (Fig. 1b).

Fig. S2 shows TRLFS spectra of $1 \cdot 10^{-5}$ M Pa(IV) in 6.0 M H_2SO_4 recorded after different times after sample preparation using two different reducing agents, Zn-Hg amalgam as rongalite. As can be seen, the rongalite provides a much longer stability of Pa(IV) than does Zn-Hg amalgam. Neither of the reducing agents seemed to influence the peak shape.

1.4 X-ray absorption spectroscopy (XAS)

Protactinium XAS measurements were performed at the INE beamline for actinide science at ANKA, Karlsruhe, Germany.[4,5] The Pa(IV) and Pa(V) sample solutions (0.3 mM Pa(IV) and Pa(V) in 6 M HCl) were filled into 200 µl capped polyethylene vials and mounted in a special air-tight sample holder, which was connected to an argon supply line at the experimental station to keep the samples under oxygen-free conditions. Note that for the XAS studies the reduction of Pa(V) to Pa(IV) was performed with Rongalite (0.8 mM) rather than Hg-Zn amalgam because Rongalite was found to hold Pa(IV) in solution for a considerably longer period of time than did Hg-Zn, see the main paper.

The XAS spectra were measured with a step width of 5 eV before the edge, 0.7 eV steps within the region -30 to 30 eV relative to the edge maximum, and thereafter with 0.03 $Å^{-1}$ equidistant steps in wave number k. Normalized and background-subtracted XAS spectra were obtained by subtraction of the pre-edge background absorption followed by normalization of the edge jump to unity. XANES and EXAFS data analysis was based on standard data reduction and least squares fit techniques using the ATHENA program package. [6] The EXAFS energy scale is transferred into wave numbers by setting the maximum of the most pronounced feature in the spectra, the so-called white line, to k = 0 $Å^{-1}$. A k range of 1.5–9.8 $Å^{-1}$ is Fourier-transformed using a Hanning window with 0.1 Å sills and theoretical fits to the data are performed in R space from 1.4–3.0 Å. Metric parameters, namely coordination numbers N (±20%), distance to neighbor atoms R (±0.02 Å) and EXAFS Debye-Waller factors σ^2 (in $Å^2$; ±20%), were determined in the fits using backscattering amplitude and phase shift functions for single scattering paths obtained from FEFF8.[1] The amplitude reduction factor S_0^2 was kept constant at 1.0 during the fit. For the single-oxygen shell fit N(O) was set to 9, while for the two-shell fit N(O) was set to 8 and σ^2(Cl) to 0.005 $Å^2$. This approach is similar to that used for U(IV) and Np(IV) in 6 M HCl solutions.[7,8]

Table S1 shows the energy positions of the first inflection point and the white line maximum of the Pa L_3-XANES of the Pa(IV) and Pa(V) solutions shown in Fig. 2a in the article. Also shown in the table is the corresponding values of Pa(IV) in aqueous HF solution.[9]

Table S2 shows the EXAFS structural fit parameters for Pa(IV) in 6 M hydrochloric acid. The results from the one-shell and two-shell fits are included. Also included are the two-shell fits for U(IV) and Np(IV) ions in 6 M hydrochloric acid taken the literature.[7,10]

Table S3 gives a compilation of published An-O distances of An(IV) aqua ions in perchloric acid or dilute hydrochloric acid solution. The table also gives the average distances used in Fig. 3 in the article.

Table S1: Energy position of the first inflection point of the rising edge and white line maximum of the Pa L_3-XANES spectra of the Pa(IV) and Pa(V) in hydrochloric and hydrofluoric acids.

Sample	First inflection point [eV]	White line maximum [eV]
$3 \cdot 10^{-4}$ M Pa(IV) in 6 M HCl[a]	16733.2	16737.3
$3 \cdot 10^{-4}$ M Pa(V) in 6 M HCl[a]	16735.2	16741.5
$1 \cdot 10^{-3}$ M Pa(V) in $5 \cdot 10^{-2}$ M HF[b]	16737.7	16741.8

[a] This study (see Fig. 2a in the main article). [b] Ref. 9.

Table S2: EXAFS structural parameters for Pa(IV), U(IV), and Np(IV) in 6 M hydrochloric acid.

Sample	shell	N	R [Å]	σ^2 [Å^2]	ΔE_0 [eV]	Reduced χ^2
$3 \cdot 10^{-4}$ M Pa(IV) in 6 M HCl[a]	O	9*	2.46(2)	0.014(3)	-0.5(2.9)	29
	O	8*	2.43(2)	0.015(5)	-2.2(6.0)	22
	Cl	1.1(8)	2.70(2)	0.005*		
$1 \cdot 10^{-2}$ M U(IV) in 6 M HCl[b]	O	7.6	2.43	0.007*	-0.4	
1st model	Cl	0.8	2.76	0.005*		
$1 \cdot 10^{-2}$ M U(IV) in 6 M HCl[b]	O	6.7	2.41#	0.007*	-1.2	
2st model	Cl	1.4	2.71#	0.005*		
$5 \cdot 10^{-3}$ M Np(IV) in 6 M HCl[c]	O	9.8	2.42	0.0075*	-7.3	
	Cl	0.6	2.71	0.004*		

[a] This study (see Fig. 2a). [b] Ref 7. [c] Ref. 8. [*] fixed parameter. [#] fixed parameter based on the results from factor analysis.

Table S3: Mean An-O bond distances (in Å) for An^{4+} aqua ions derived from EXAFS and HEXS studies.[a]

An-O	Average An-O distance	An-O distances reported
Th-O	2.453(10)	2.45(1),[10] 2.45(1),[11] 2.451(3),[12] 2.46(1)[13]
Pa-O	2.43(2)	2.43(2) [b]
U-O	2.415(10)	2.40(1),[14] 2.42(1)[11]
Np-O	2.40(1)	2.40(1),[8] 2.40(1)[15]
Pu-O	2.385(10)	2.38(1),[16] 2.39(2)[17]
Bk-O	2.32(1)	2.32(1)[35]

[a] Uncertainties are given within brackets. [b] This study.

2. Quantum chemical calculations

Small-core relativistic effective core potentials of the Stuttgart-Cologne group were employed for all actinide elements,[18] along with the segmented basis sets,[19] corresponding to the following contraction (14s13p10d8f1g) / [10s9p5d4f1g]. Augmented correlation-consistent polarization valence triple-ζ (aug-cc-pVTZ) basis sets were used for oxygen,[20] and hydrogen atoms.[21] The structures of the various isomers were optimized without symmetry constraints at the restricted MP2 level (Th(IV)) and unrestricted (Pa(IV), U(IV), Np(IV), Pu(IV)) high-spin MP2 level (Table S6) using the parallel resolution of the identity approximation,[22] with the appropriate atomic auxiliary basis functions.[23,24] Harmonic frequency calculations were computed numerically at the optimized geometry, at the MP2 or UMP2 level, not only to confirm that the optima found correspond to energy minima, but also to compute the vibrational partition functions at 298.15 K and 0.1 MPa, which are necessary to calculate the enthalpic and entropic contributions to the gas-phase energies. For the open 5*f*-shell systems, Pa(IV), U(IV), Np(IV), Pu(IV), the ground-state electronic configuration might exhibit a multi-reference character because of spin-orbit coupling within the nearly degenerate 5*f* orbitals. Density functional theory (DFT) methods are not suited in this context for two reasons: 1) Kohn-Sham DFT being a single-determinant based theory, it cannot describe the inherent multi-configurational nature of electronic ground state of open-shell actinide elements; 2) with the current functionals, tends to overestimate heavy-metal-ligand interactions.[25] We have therefore performed multi-reference CASPT2 calculations distributing one to four unpaired electrons in the seven 5*f* orbitals. In the MP2 and CASPT2 calculations, the 1*s* core orbitals of the oxygen atoms, and 5*s*, 5*p*, 5*d* orbitals of the actinide ions were kept frozen. In order to estimate the spin-orbit coupling effects on the gas-phase energies, single-point calculations were computed at the previously correlated optimized geometries with the Restricted Active Space State Interaction (RASSI) approach,[26] using all-electron atomic natural orbitals relativistic core correlation basis sets (ANO-RCC) with triple-zeta contractions for all atoms.[27] All spin-states corresponding to a given f^n (n=1,4) configuration were coupled, this corresponds to 7 doublet states for Pa(IV), 21 triplet and 28 singlet states for U(IV), 35 quartet and 122 doublet states for Np(IV), 35 quintet, 210 triplet and 196 singlet states for Pu(IV), 21 sextet, 224 quartet, 490 doublet states for Am(IV), 140 quintets, 588 triplet, 490 singlet states for Cm(IV), 1 octet, 48 sextet, 392 quartet, 784 doublet states for Bk(IV). The spin-orbit integrals were computed in the mean field approximation using the AMFI code implemented in the MOLCAS suite of programs.[28, 29] The contribution of hydration to the free energies of all isomers was estimated by single-point COSMO calculations with a dielectric constant of 78.9.[29] To reduce the uncertainties of the COSMO calculations,[30] a B3LYP based density and small def2-SVP basis sets[31] on all atoms are used. The COSMO solvation free energies are corrected with the "explicit hydrogen bond correction" (EHBC) of $\Delta E = -6.97 \times \Delta k$ kJ/mol, where Δk is the change in the number of hydrogen bonds between the various isomers.[32] The correction amounts to -13.94 kJ/mol for the relative energy between the eight and nine-coordinated isomers, and +13.94 kJ/mol for that between the ten and nine-coordinated isomers. All MP2 and COSMO calculations are performed with the Turbomole 6.4 quantum chemistry package,[33] while multi-reference CASPT2 and SO-CASPT2 calculations were run with the MOLCAS7.8 quantum chemistry package. To analyze the nature of the actinide-water chemical bond the quantum theory of atoms-in-molecules (QTAIM) analysis, we used the Gaussian 09 (Revision C01) quantum

chemistry package,[34] with the same basis sets, which provides the appropriate wave-function extended files (wfx) to be used by the AIMAll package.[35]

Table S4. Calculated mean and structural standard deviations for the An-O bond distances (in Å) in the $[An(H_2O)_{10-n}]^{4+}\cdot(H_2O)_n$ (n = 0-2) clusters.

	$[An(H_2O)_{10}]^{4+}$	$[An(H_2O)_9]^{4+}\cdot H_2O$	$[An(H_2O)_8]^{4+}\cdot(H_2O)_2$
Th-O	2.551±0.020	2.506±0.031	2.466±0.018
Pa-O	2.518±0.026	2.471±0.034	2.429±0.016
U-O	2.491±0.043	2.443±0.039	2.400±0.022
Np-O	2.472±0.033	2.425±0.039	2.383±0.025
Pu-O	2.454±0.023	2.406±0.032	2.361±0.020
Am-O	2.444±0.027	2.393±0.038	2.347±0.016
Cm-O	2.435±0.013	2.385±0.046	2.339±0.034
Bk-O	2.434±0.059	2.374±0.059	2.329±0.015

Table S5. QTAIM charge (Q(M)) and the electron density (ρ_b), Laplacian ($\nabla^2\rho_b$), and the energy density (H_b) at the An-O bond critical point.

	Q(M)	ρ_b [e^-/bohr^3]	$\nabla^2\rho_b$ [e^-/bohr^5]	H_b [au]
Th	3.41	0.051	0.194	-0.0033
Pa	3.44	0.052	0.223	-0.0026
U	3.29	0.055	0.226	-0.0044
Np	3.31	0.057	0.239	-0.0045
Pu	3.29	0.058	0.248	-0.0049
Am	3.27	0.059	0.253	-0.0051
Cm	3.26	0.059	0.255	-0.0050
Bk	3.27	0.059	0.260	-0.0048

Table S6. Spin-orbit lowering (in kJ/mol) in the bare An^{4+} ion and in the $[An(H_2O)_{10-n}]^{4+}\cdot(H_2O)_n$ (n = 0-2) clusters. Being a closed-shell system, thorium has negligible spin-orbit coupling contributions.

	An^{4+}	$[An(H_2O)_8]^{4+}\cdot(H_2O)_2$	$[An(H_2O)_9]^{4+}\cdot H_2O$	$[An(H_2O)_{10}]^{4+}$
Pa	-43.6	-34.3	-32.2	-31.8
U	-89.6	-78.0	-76.1	-77.3
Np	-128.0	-112.3	-114.8	-112.7
Pu	-153.3	-142.7	-140.2	-136.3
Am	-177.2	-157.1	-163.7	-159.5
Cm	-197.8	-175.3	-181.0	-167.7
Bk	-24.6	-26.6	-28.0	-28.3

Table S7. Relative electronic energies of the $[An(H_2O)_{10}]^{4+}$, $[An(H_2O)_9]^{4+}\cdot H_2O$, and $[An(H_2O)_8]^{4+}\cdot(H_2O)_2$ clusters for An = Th-Bk, without (ΔG) and with (ΔG^{corr}) the hydrogen bond correction of -6.97 kJ/mol, per hydrogen bonds.[a]

	$[An(H_2O)_8]^{4+}\cdot(H_2O)_2$		$[An(H_2O)_9]^{4+}\cdot H_2O$		$[An(H_2O)_{10}]^{4+}$	
	ΔE	ΔE^{corr}	ΔE	ΔE^{corr}	ΔE	ΔE^{corr}
Th	27.5	13.6	0.0	0.0	7.9	21.9
Pa	20.7	6.9	0.0	0.0	18.5	32.5
U	18.6	4.7	0.0	0.0	19.0	32.9
Np	18.1	4.1	0.0	0.0	24.0	37.9
Pu	14.0	0.0	0.0	0.0	29.2	43.1
Am	17.5	3.6	0.0	0.0	38.9	52.8
Cm	12.3	-1.7	0.0	0.0	44.1	58.0
Bk	15.2	1.2	0.0	0.0	48.9	62.9

[a] All values are at the SO-CASPT2 level, except for the closed-shell Th(IV) complexes, for which MP2 energies were used; long-range hydration effects were accounted for with the COSMO solvent model, without or with the hydrogen bond correction.

Table S8. Total free energies in atomic units in the $[An(H_2O)_{10-n}]^{4+}\cdot(H_2O)_n$ (n = 0-2) clusters including CASPT2 dynamical correlation, spin-orbit effets, thermodynamical corrections and COSMO solvent effects.

	$[An(H_2O)_8]^{4+}\cdot(H_2O)_2$	$[An(H_2O)_9]^{4+}\cdot H_2O$	$[An(H_2O)_{10}]^{4+}$
Th	-1169.3732683	-1169.3828840	-1169.3814857
Pa	-1202.9827452	-1202.9897726	-1202.9833894
U	-1238.4888196	-1238.4951578	-1238.4860684
Np	-1275.9191802	-1275.9259584	-1275.9160376
Pu	-1315.3289958	-1315.3347533	-1315.3222139
Am	-1356.9002942	-1356.9060195	-1356.8914243
Cm	-1400.4815630	-1400.4848593	-1400.4680704
Bk	-1446.2199613	-1446.2235380	-1446.2067385

References for Supplementary Information

1 D. Brown, A. J. Smith, R. G. Wilkins, *J. Chem. Soc*., 1959, 1463-1466

2 a) S. Fried and J. C. Hindmann, *J. Am. Chem. Soc.,* 1954, **76**, 4863-4864; b) T. Mitsuji, *Bulletin of the Chemical Society of Japan*, 1967, **40**, 2091-2095; c) M. Haïssinsky and G. Bouissières, *Compt. Rend. Acad. Sci. Paris*, 1948, **226**, 573–594; d) C. Keller, *Angew. Chem. Int. Ed.*, 1966, **5**, 23-33.

3 G. Bernhard, G. Geipel, V. Brendler and H. Nitsche, *Radiochim. Acta,* 1996, **74**, 87–91.

4 B. Brendebach, N. L. Banik, C. M. Marquardt, J. Rothe, M. Denecke and H. Geckeis, *Radiochimica Acta.*, 2009, **97**, 701-708.

5 J. Rothe, S. Butorin, K. Dardenne, M. A. Denecke, B. Kienzler, M. Löble, M.; V. Metz, A. Seibert, M. Steppert, T. Vitova, C. Walther and H. Geckeis, *Rev. Sci. Instrum*., 2012, **83**, 043105.

6 B. Ravel, M. Newville, *J. Synchrotron Rad.*, 2005, **12**, 537.

7 C. Hennig, J. Tutschku, A. Rossberg, G. Bernhard, A. C. Scheinost, *Inorg. Chem*., 2005, **44**, 6655-6661.

8 P. G. Allen, J. J. Bucher, D. K. Shuh, N. M. Edelstein and T. Reich, *Inorg. Chem*., 1997**, 36,** 4676-4683.

9 C. Hennig, C. Le Naour and C. Den Auwer, *Phys. Rev. B.*, 2008, **77**, 235102.

10 V. Neck, R. Müller, M. Bouby, M. Altmaier, J. Rothe, M. A. Denecke and J. I. Kim, *Radiochim. Acta.*, 2002, **90**, 485–494.

11 H. Moll, M. A. Denecke, F. Jalilehvand, M. Sandström and I. Grenthe, *Inorg. Chem.*, **1999**, **38***,* 1795-1799.

12 N. Torapava, I. Persson, L. Eriksson and D. Lundberg, *Inorg. Chem*., 2009, **48**, 11712-11723.

13 R. E. Wilson, S. Skanthakumar, P. C. Burns, L. Soderholm, *Angew. Chem. Int. Ed*., 2007, **46**, 8043-8045.

14 A. Ikeda-Ohno, C. Hennig, S. Tsushima, A. C. Scheinost, G. Bernhard and T. Yaita, *Inorg. Chem*., 2009, **48**, 7201-7210.

15 A. Ikeda-Ohno, C. Hennig, A. Rossberg, H. Funke, A. C. Scheinost, G. Bernhard, T. Yaita, *Inorg. Chem.*, 2008, **47**, 8294-8305.

16 J. Rothe, C. Walther, M. A. Denecke and T. Fanghänel, *Inorg. Chem.*, 2004, **43,** 4708-4718.

17 K. Dardenne, A. Seibert, M. A. Denecke and C. M. Marquardt, *Radiochim. Acta*, 2009, **97**, 91-97.

18 W. Küchle, M. Dolg, H. Stoll and H. Preuss, *J. Chem. Phys.*, 1994, **100**, 7535-7542.

19 a) X. Cao and M. Dolg, *J. Chem. Phys.*, 2004, **673***,* 203–209; b) X. Cao, M. Dolg and H. Stoll, *J. Chem. Phys.* 2003, **118***,* 487-496.

20 D. E. Woon and T. H. Dunning, *J. Chem. Phys.*, 1994, **100**, 2975.

21 T. H. Dunning, Jr. *J. Chem. Phys.*, 1989, **90**, 1007.

22 a) C. Hättig, A. Hellweg and A. Köhn, *Phys. Chem. Chem. Phys.*, 2006, **8**, 1159–1169; b) C. Hättig and F. Weigend, *J. Chem. Phys.*, 2000, **113**, 5154–5161.

23 F. Weigend, A. Köhn and C. Hättig, *J. Chem. Phys.*, 2002, **116**, 3175–3183.

24 C. Hättig, *Phys. Chem. Chem. Phys.*, 2005, **7**, 59–66.

25 a) K. E. Gutowski and D. A. Dixon, *J. Phys. Chem. A*, 2006, **110**, 8840–8856; b) P. Wåhlin, C. Danilo, V. Vallet, F. Réal, J.-P. Flament and U. Wahlgren, *J. Chem. Theory Comput.*, 2008, **4**, 569–577; c) J. P. Austin, N. A. Burton, I. H. Hillier, M. Sundararajan and M. A. Vincent, *Phys. Chem. Chem. Phys.*, 2009, **11**, 1143–1145; d) F. Réal, M. Trumm, V. Vallet, B. Schimmelpfennig, M. Masella and J.-P. Flament, *J. Phys. Chem. B*, 2010, **114**, 15913–15924.

26 P.-Å Malmqvist, B. O. Roos and B. Schimmelpfennig, *Chem. Phys. Lett.*, 2002, **357**, 230.

27 B. O. Roos, R. Lindh, P.-Å. Malmqvist, V. Veryazov, P.-O. Widmark, *J. Phys. Chem. A*, 2004, **108**, 2851.

28 B. Schimmelpfennig, AMFI, an Atomic Mean-Field Integral program.

29 G. Karlström, R. Lindh, P.- Å. Malmqvist, B. O. Roos, U. Ryde, V. Veryazov, P.-O. Widmark, M. Cossi, B. Schimmelpfennig, P. Neograd y and L. Seijo, *Comput. Mater. Sci.*, 2003, **28**, 222–239; b) V. Veryazov, P. O. Widmark, L. Serrano-Andr´es, R. Lindh and B. O. Roos, Int. J. Quant. Chem., 2004, 100, 626; c) F. Aquilante, L. De Vico, N. Ferré, G. Ghigo, P.-Å. Malmqvist, P. Neogrády, T. B. Pedersen, M. Pitonak, M. Reiher, B. O. Roos, L. Serrano-Andrés, M. Urban, V. Veryazov and R. Lindh, *J. Comput. Chem.*, 2010, **31**, 224–247.

30 A. Klamt, G. Schüürmann, *J. Chem. Soc. Perkin Trans.*, 1993, **2***,* 799.

31 R. Ahlrichs, M. Bär, M. Häser, H. Horn, C. Kölmel, *Chem. Phys. Lett.*, 1989**, 162***,* 165–169.

32 N. Heinz, J. Zhang and M. Dolg, *J. Chem. Theory Comput.*, 2014, **10**, 5593–5598.

32 TURBOMOLE V6.4 2012, a development of University of Karlsruhe and Forschungszentrum Karlsruhe GmbH, **1989-2007**, TURBOMOLE GmbH, since 2007; available from http://www.turbomole.com.

33 M. J. Frisch, et al. Gaussian 09, revision C.01; Gaussian, Inc.: Wallingford, CT, **2009**.

34 AIMAll (Version 12.06.21), Todd A. Keith, TK Gristmill Software, Overland Park KS, USA, 2012 (aim.tkgristmill.com).

35 M. R. Antonio, C. W. Clayton, L. Soderholm, *Radiochim. Acta,* 2002, **90**, 851-856.